Journal of Molecular Graphics and Modelling 55 (2015) 25–32

Contents lists available at ScienceDirect

Journal of Molecular Graphics and Modelling

journal homepage: www.elsevier.com/locate/JMGM

Theoretical study of the mechanism of protein arginine deiminase 4 (PAD4) inhibition by F-amidine

Dongmei Li[a,b,*], Cui Liu[a,b], Jianping Lin[a,b,*]

[a] State Key Laboratory of Medicinal Chemical Biology and College of Pharmacy, Nankai University, Tianjin 300071, China
[b] Tianjin Key Laboratory of Molecular Drug Research, Nankai University, Tianjin 300071, China

ARTICLE INFO

Article history:
Accepted 27 October 2014
Available online 7 November 2014

Keywords:
PAD4
QM/MM
ONIOM
Transition state
Protonation state

ABSTRACT

Protein arginine deiminase 4 (PAD4) catalyzes the hydrolysis of a peptidylarginine residue to form a citrulline residue and ammonia during posttranslational modification. This process plays a pivotal role in rheumatoid arthritis (RA) and gene regulation. F-amidine belongs to a series of haloacetamidine compounds that are the most potent PAD4 inhibitors described to date. F-amidine acts as a mechanism-based inhibitor of PAD4, inactivating PAD4 by the covalent modification of the active site Cys645. In this manuscript, the fundamental mechanism of PAD4 inhibition by F-amidine is investigated using a QM/MM approach. Our simulations show that in the PAD4–F-amidine reactant complex, the active site Cys645 exists as a thiolate and His471 is protonated. This is consistent with the reverse protonation mechanism wherein the active site nucleophile, Cys645, in PAD4 exists as a thiolate in the active form of the enzyme. Inhibition of PAD4 by F-amidine is initiated by the nucleophilic addition of S_γ to the C_ζ of F-amidine, leading to the formation of a tetrahedral intermediate. His471 serves as a proton donor, helping F to leave the fluoroacetamidine moiety of F-amidine; meanwhile, S_γ forms a three-membered ring with C_ζ and C_η of F-amidine. Subsequently, the three-membered sulfonium ring collapses and rearranges to the final thioether product. His471 acts as a proton donor in the transition state and facilitates the inhibition reaction of PAD4.

1. Introduction

Protein arginine deiminase 4 (PAD4) catalyzes the conversion of the peptidylarginine residue to citrulline residue and ammonia [1,2]. PAD4 has attracted significant attention in the past several years because of its presumed role as a causative factor in the pathophysiology of rheumatoid arthritis (RA) [3,4]. In addition, PAD4 behaves as a transcriptional coregulator in the post-translational modification process by deiminating multiple transcriptional regulators, including p300 and histones H2A, H3, and H4 [5,6]. PAD4 belongs to a superfamily of Arg-modifying enzymes (e.g., arginine deiminase (ADI) [7] and dimethylamine dimethylarginine hydrolase (DDAH) [8,9]) and shares a common two-stage catalytic mechanism consisting of a deimination stage and a hydrolysis stage. In the deimination stage, the active site Cys645 attacks the guanidinium carbon (C_ζ) of the arginine residue, generating a first tetrahedral intermediate; the C_ζ—$N_{\eta1}$ bond then cleaves and releases a molecule of ammonia. In the hydrolysis stage, His471 activates a water molecule that attacks the C_ζ of the first tetrahedral intermediate to form a second tetrahedral intermediate; the S_γ—C_ζ bond then breaks to generate the final product, citrulline [10–12].

Because of PAD4's significant role in transcriptional regulation and its potential role in causing RA, significant work has aimed to develop PAD4 inhibitors to modulate PAD4 activity and RA progression [13–19]. Among the identified PAD4 inhibitors, taxol [13], streptomycin and minocycline [14] are reversible; however, these compounds have millimolar IC_{50} values and are thus relatively weak inhibitors. The most potent inhibitors described to date are a series of haloacetamidine compounds (e.g., F-amidine, Cl-amidine and their analogs; IC_{50} = 1.9–22 μM) [16–19] developed by Thompson and co-workers. The structures of F-amidine and Cl-amidine are similar to that of benzoyl-L-arginine amide (BAA), a small molecule substrate of PAD4, except that they incorporate a reactive haloacetamidine moiety in place of the substrate guanidinium. F-amidine and Cl-amidine are active against PAD4 in vitro and in cells [16,17]. Additionally, Cl-amidine has been shown to reduce disease severity in mouse

* Corresponding authors at: College of Pharmacy, Nankai University, Tianjin 300071, China. Tel.: +86 22 23506290.
E-mail addresses: dongmeili@nankai.edu.cn (D. Li), jianpinglin@nankai.edu.cn (J. Lin).

http://dx.doi.org/10.1016/j.jmgm.2014.10.014
1093-3263/

models of RA [20]. Recently, Wang et al. reported a Cl-amidine analog, YW3-56, where the N_α-benzoyl and C_α-amide groups in Cl-amidine were replaced with dimethylamide-naphthalene and benzylamide groups, respectively, resulting in improved bioavailability [21]. These haloacetamidine compounds act as mechanism-based inhibitors of PAD4. The high PAD4 inhibition activity of haloacetamidine suggests that these compounds are powerful small molecule chemical probes that can be used to discern the normal and pathophysiological roles of PAD4 and study how dysregulation of these pathways contributes to the onset and progression of RA. Because F-amidine links covalently to PAD4 to inhibit it [17], F-amidine has been converted to a robust activity-based protein-profiling reagent (ABPP) [22] by the addition of a fluorophore. Such a compound can be useful to identify the in vivo conditions under which PAD4 is activated and to isolate activated PAD4.

To elucidate the mechanism by which F-amidine inhibits PAD4 is of fundamental importance as well as significant medical interest for the rational design of highly active mechanism-based inhibitors of PAD4. Much work has been done to characterize the mechanism of PAD4 inhibition by F-amidine [16,17,23]. Crystallographic data confirms that PAD4 inactivation is due to the covalent modification of the active-site Cys645 [17]. Mechanistic studies with F-amidine show bell-shaped pH inactivation rate profiles for PAD4 (in the pH range 6.0–8.0); the drop in the inactivation rate at higher pH values (~8.1) indicates that general acid catalysis promotes enzyme inhibition after the formation of the initial enzyme-inhibitor complex. Based on these results, Thompson and co-workers recently proposed that the inhibition of PAD4 by F-amidine occurs via the initial attack of the Cys645 thiolate on the amidinium carbon, resulting in the formation of a stable tetrahedral intermediate. The halide displacement reaction then proceeds to generate a three-membered sulfonium ring. Collapse of the three-membered ring leads to a 1,2-shift, generating a thioether adduct. Their data further suggest that the protonation of the tetrahedral intermediate helps to drive F-displacement to form the three-membered sulfonium ring, which ultimately collapses to form the inactivated enzyme; His471 is the likely proton donor [23].

For rational design of novel inhibitors of PAD4, it is important to understand the detailed mechanism concerning how the enzyme is inhibited. A detailed understanding of the mechanism of PAD4 inhibition could provide a valuable mechanistic base for rational design of a possible stable analog of the rate-determining transition state as a novel type of PAD4 inhibitor. To elucidate the reactant complex of PAD4 and F-amidine, and to understand the molecular mechanism about the inhibition, we performed molecular dynamics simulations and QM/MM calculations on the PAD4 inhibition by F-amidine. Two probable states were examined: State I, in which Cys645 is deprotonated and His471 is charged, and State N, in which both Cys645 and His471 are neutral (Scheme 1). Our calculations indicated that in the PAD4–F-amidine reactant complex, the active site Cys645 exists as a thiolate and His471 is protonated. The inhibition of PAD4 by F-amidine was initiated by the nucleophilic addition of S_γ to the C_ξ of F-amidine, and the reaction proceeded through a three-membered sulfonium ring transition state. His471 acted as a proton donor in the transition state, facilitating the inhibition process.

2. Computational methods

2.1. Protein setup and MD simulations

A crystal structure of PAD4 (PDB code 2DW5) inhibited by F-amidine was selected as the initial structure for our study [17]. Because the *N*-terminal domain of PAD4 is far from the active site and does not affect the catalytic function of PAD4 [24], residues Met1 to Ala294 and their surrounding water and ions were removed to reduce computational cost. Fig. 1 shows the active-site structure of the F-amidine and PAD4 covalent complex, which corresponds to the product of the inhibition reaction. We split the covalent bond between F-amidine and Cys645 and modified the geometry of the ligand to prepare the geometry for a Michaelis reactant complex, namely, the pre-reaction state. Both State I and State N models of PAD4, which differ in the protonation states for Cys645 and His471, were prepared with the same procedure and equilibrated with the same simulation protocol. Hydrogen atoms were added by Leap in the Amber 11 package [25]. Cys645 is deprotonated and His471 is charged for PAD4 in State I, while Cys645 is protonated and His471 is neutral as HIE in State N. The local hydrogen bond network was carefully checked in determining the protonation states of all other histidine residues: His644 was identified to be protonated as HIP because it forms two hydrogen bonds with Asp473 and a crystal water, while all other histidine residues are neutral. The ligand atomic charges were determined by the restrained electrostatic potential (RESP) method using Gaussian 03 [26] and Antechamber [27]; the geometries of the ligand were optimized at the B3LYP/6-31G* level [28–30]. The resulting complex of PAD4 and F-amidine was neutralized by adding seven Cl^- counterions and solvated in a periodic TIP3P rectangular water box with a buffer distance of 10 Å between each wall and the closest atom in each direction. This generated a simulation system consisting of ~48,000 atoms for both State I and State N.

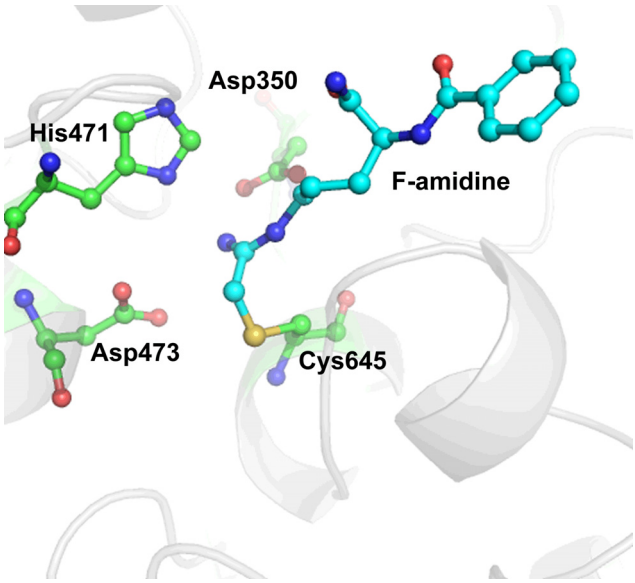

Fig. 1. X-ray structure of PAD4 complexed with F-amidine (PDB code 2DW5).

After the system was generated, the hydrogen atoms were minimized for 2000 steps, the position of water molecules and ions were minimized for 5000 steps, the side chains of PAD4 were minimized for 5000 steps and the entire system was finally minimized for 10,000 steps. Energy minimizations were performed using the steepest descent algorithm for the first 500 steps and the conjugated gradient algorithm for the remaining steps. After the series of minimizations, the system was gradually heated from 10 to 298.15 K in 50 ps followed by a MD simulation at 298.15 K for 3 ns. Minimizations and MD simulations with periodic boundary conditions were conducted with the Sander module of Amber 11 [25]. The AMBER99SB force field [31,32] was employed for the protein, while the general AMBER force field (GAFF) [33] was used for the ligand. A 10-Å cutoff was used for nonbonded interactions, and the nonbonded list was updated every 500 steps. The SHAKE algorithm [34]

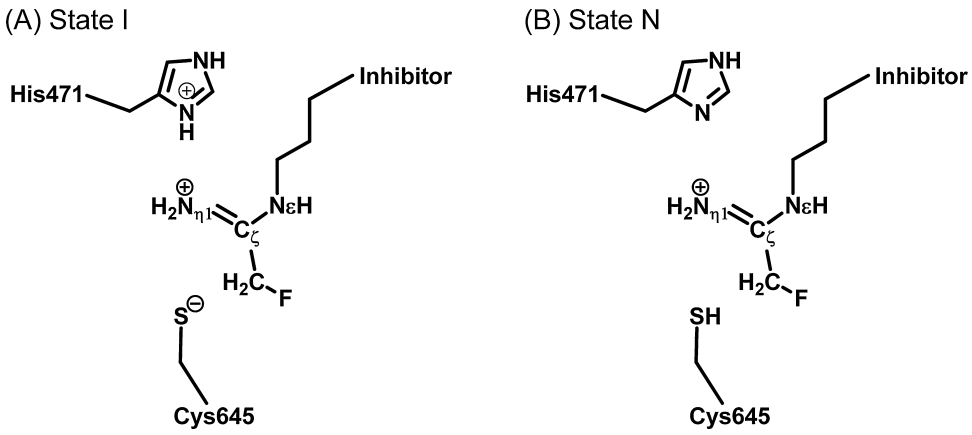

Scheme 1. State I and State N of the system.

was employed to constrain all covalent bonds involving hydrogen atoms, enabling the use of a 2-fs time step to numerically integrate the equations of motion. The particle mesh Ewald method [35] was applied to treat long-range electrostatic interactions.

2.2. QM/MM calculations

The trajectories for both State I and State N are quite stable. For each state, a representative snapshot close to the average simulated structure was extracted from the stable trajectory as the starting structure for the QM/MM calculation. Snapshots at 2.976 ns and 2.939 ns were taken from State I and State N, respectively. Prior to QM/MM calculations, each selected starting structure was minimized for 5000 steps using a constraint with a 500 kcal/(mol Å^2) force constant to constrain the reactive center (F-amidine, Cys645, His471 and Asp473). With the minimized starting structure, the QM/MM system was obtained by removing water molecules beyond 30 Å of the F-amidine C_ζ atom. The resulting QM/MM system contained 12,801 atoms for State I and 12,651 atoms for State N. The QM/MM partition is illustrated in Fig. 5A. Fragments directly involved in the reaction, including side chains of Cys645, His471, Asp473, and the ligand F-amidine, were defined as QM atoms, while the remaining atoms were defined as the MM part. The QM/MM calculations were performed with the ONIOM method [36–38] implemented in Gaussian 09 [39]. During the QM/MM optimization, any residues containing an atom within 20 Å of the F-amidine C_ζ atom were allowed to move, while atoms outside this range were frozen, resulting in 4433 movable atoms for the State I system and 4606 movable atoms for the State N system. Geometry optimization was performed with the mechanical embedding scheme method of ONIOM (ONIOM-ME) at the B3LYP/6-31G:AMBER level. Frequency calculations at the same level were also performed to verify the reactants, transition states, intermediates, and final products. The optimized geometries were used to carry out single-point calculations with the electronic embedding scheme (ONIOM-EE) method at the B3LYP/6-311++G**:AMBER level and MP2/6-311++G**:AMBER level.

3. Results and discussion

3.1. Protonation states of the active site residues

The most controversial issue regarding PAD4 involves the protonation states of the active site residues in the reactant complex. Experimental work by Thompson and co-workers revealed that the PAD4 uses a reverse protonation mechanism wherein the active site nucleophile, Cys645, exists as a thiolate in the active form of the enzyme [11]. In contrast, QM/MM MD simulations by Zhang and co-workers suggested that the nucleophilic species is the thiol form of Cys645 [40,41]. We examine two probable states, State I and State N; both complexes are stable during the MD simulations with RMSD values of 1.08 Å and 1.01 Å, respectively. The nucleophilic Cys645 is located beside the fluoroacetamidine moiety of F-amidine. As seen in Fig. 2, the average distance between the S_γ of Cys645 and the C_ζ of F-amidine is 3.15 Å in State I and 3.35 Å in State N. In both complexes, the S_γ of Cys645 is close enough to attack the fluoroacetamidine moiety of F-amidine.

MD simulations resulted in dynamically stable complexes of PAD4 and F-amidine in both State I and State N. These stable

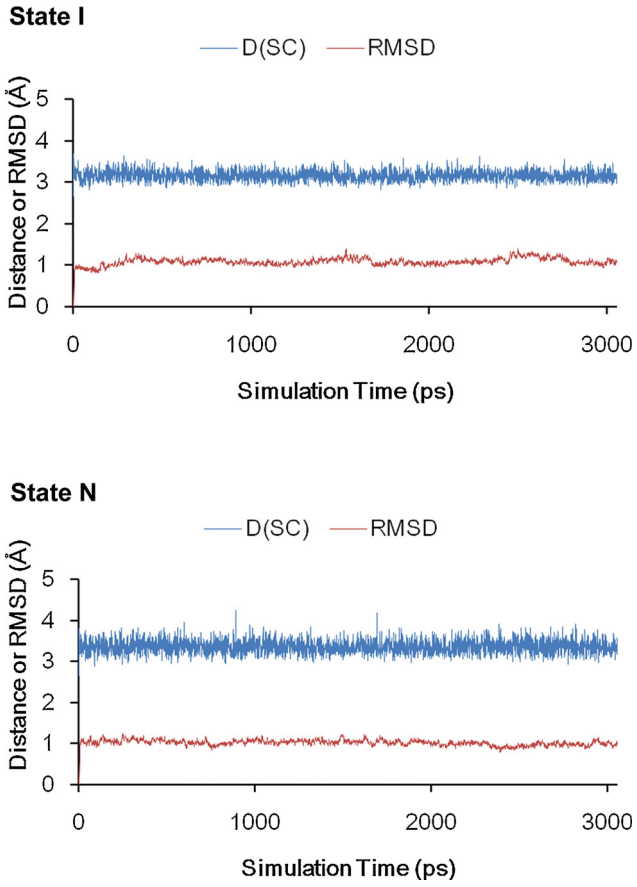

Fig. 2. Distances between the S_γ of Cys645 and the C_ζ of F-amidine along with RMSD values for PAD4 backbone atoms during the MD simulations of State I and State N.

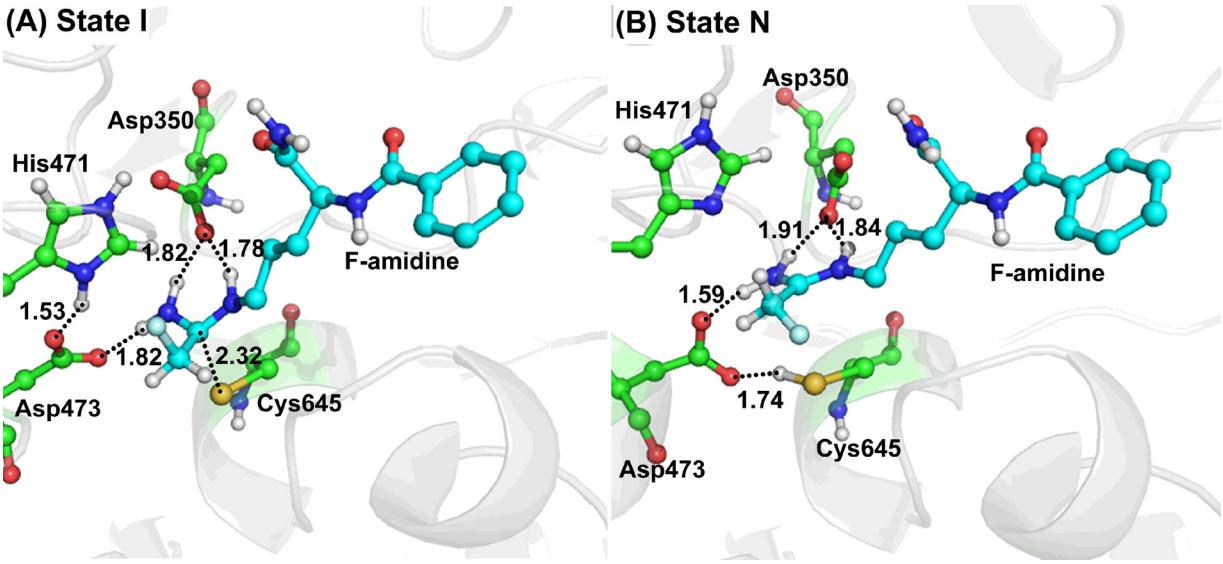

Fig. 3. QM/MM optimized geometries (bond distances in Å) of (A) State I and (B) State N.

reactant complexes were chosen as the starting points for QM/MM reaction coordinate calculations for the two states. Fig. 3 shows the QM/MM optimized geometries of State I and State N. A previous QM/MM MD simulation of PAD4 with its substrate histone H4 indicated an unstable active site in State I, which causes the substrate to drift out of the active site and disrupt the enzyme–substrate complex [40]. In contrast, our QM/MM calculation of State I shows that the inhibitor F-amidine is held tightly by three hydrogen bonds with Asp350 and Asp473 in the active site of PAD4, and Asp437 also forms a hydrogen bond with His471 (see Fig. 3A). These hydrogen bond interactions are similar to those in the crystal structure of C645A mutant with BAA [42] (PDB code 1DWA), which corresponds to the reactant complex of the inhibition process. In 1DWA, both $O_{\delta1}$ and $O_{\delta2}$ of Asp350 form hydrogen bonds with the N_{ε} and $N_{\eta1}$ of BAA, and the carboxyl group of Asp473 forms two hydrogen bonds with both $N_{\eta1}$ and $N_{\eta2}$ of the substrate (see Fig. S1). Because the guanidinium of BAA is replaced with haloacetamidine in F-amidine, the hydrogen bond between the O_{δ} of Asp473 and the $N_{\eta2}$ of BAA is lost in the PAD4–F-amidine complex. The S_{γ} of Cys645 is positioned at a distance of 2.32 Å below the C_{ζ} of F-amidine. Overall, we see that the active site residues are well orientated for the nucleophilic attack of S_{γ} to the C_{ζ} of F-amidine.

In State N, the hydrogen bond interactions between the fluoroacetamidine moiety of F-amidine and Asp350 and Asp473 are similar to those in State I (e.g., the carboxyl group of Asp350 forms two hydrogen bonds with N_{ε} and N_{η} of F-amidine, and the carboxyl group of Asp473 forms a hydrogen bond with N_{η} of F-amidine). The SH proton of Cys645 points toward the $O_{\delta1}$ of the Asp473 carboxyl group, forming a hydrogen bond with a S_{γ}—H. . .$O_{\delta1}$ distance of 1.74 Å. Due to this short S_{γ}—H. . .$O_{\delta1}$ distance, the thiol proton of Cys645 can be easily transferred to the carboxyl group of Asp473, and the resulting deprotonated thiolate can nucleophilically attack the C_{ζ} of F-amidine.

To compare the stability of State I and State N, we employed QM/MM reaction coordinate calculations for the transformation from State I to State N. Fig. 4 shows the energy profile of the transformation. The calculated energy barrier for the transformation is 26.9 kcal/mol at the ONIOM-EE B3LYP/6-311++G**:AMBER level and 28.3 kcal/mol at the ONIOM-EE MP2/6-311++G**:AMBER level. Our calculations suggest that transformation from State I to State N proceeds in a stepwise manner. In the first step, His471 transfers the proton from its N_{δ} to the N_{η} of F-amidine; meanwhile, F-amidine transfers another proton from its N_{η} to the $O_{\delta1}$ of Asp473. In the second step, Asp473 transfers the proton obtained in the first step from its $O_{\delta1}$ to the S_{γ} of Cys645; the negatively charged S_{γ} of Cys645 is then protonated, which corresponds to the neutral State N. The second step is rate-determining.

The optimized geometries of State I, transition states (TS), intermediate (INT), and product (PC_I) are depicted in Fig. 5. In State I, the N_{δ} of His471 forms a hydrogen bond with the $O_{\delta2}$ of Asp473 (with a N_{δ}—H. . .$O_{\delta2}$ distance of 1.53 Å), and the $O_{\delta1}$ of Asp473 forms a hydrogen bond with the N_{η} of F-amidine (with a $O_{\delta1}$. . .H—N_{η} distance of 1.82 Å). In the geometry of the first transition state, TS_1, the proton on the His471 N_{δ} transfers to the N_{η} of F-amidine (with a N_{δ}. . .H distance of 1.23 Å and a H. . .N_{η} distance of 1.40 Å). Meanwhile, another proton on the N_{δ} of His471 transfers to the $O_{\delta1}$ of Asp473 (with a N_{δ}. . .H distance of 1.08 Å and a H. . .$O_{\delta1}$ distance of 1.63 Å). In the geometry of intermediate, INT, where the two concerted hydrogen-transfers occurred, the deprotonated N_{δ} of His471 forms a hydrogen bond with the N_{η} of F-amidine (with a N_{δ}. . .H—N_{η} distance of 1.88 Å), and the N_{η} of His471 forms a hydrogen bond with the $O_{\delta1}$ of Asp473 (with a N_{η}—. . .H—$O_{\delta1}$ distance

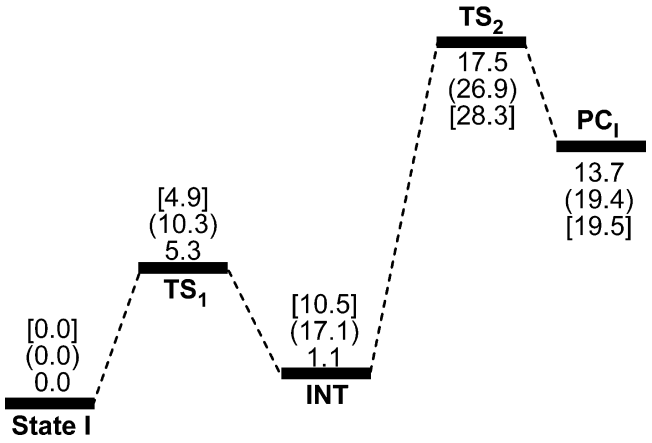

Fig. 4. Energy profile for the transformation from State I to State N. The relative energies (in kcal/mol) include zero-point corrections and correspond to different levels: ONIOM-ME B3LYP/6-31G:AMBER (no parentheses), ONIOM-EE B3LYP/6-311++G**:AMBER (in parentheses) and ONIOM-EE MP2/6-311++G**:AMBER (in square brackets).

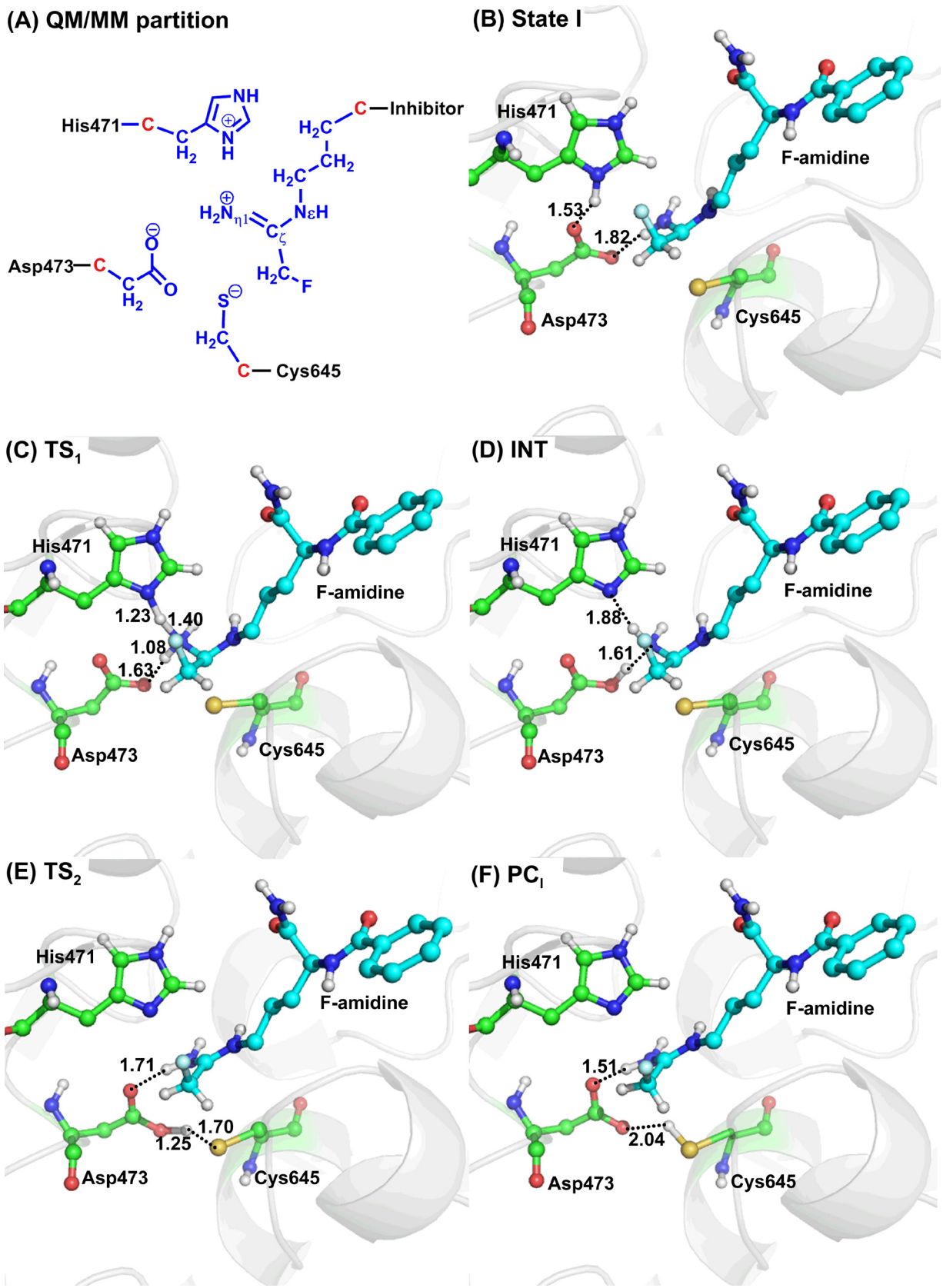

Fig. 5. (A) QM/MM partition of State I. QM atoms are colored blue, boundary atoms are colored red, and all other atoms belong to the MM subsystem. (B–F) Optimized geometries (bond distances in Å) of key configurations during the transformation from State I to State N. (For interpretation of the references to color in this figure legend, the reader is referred to the web version of this article.)

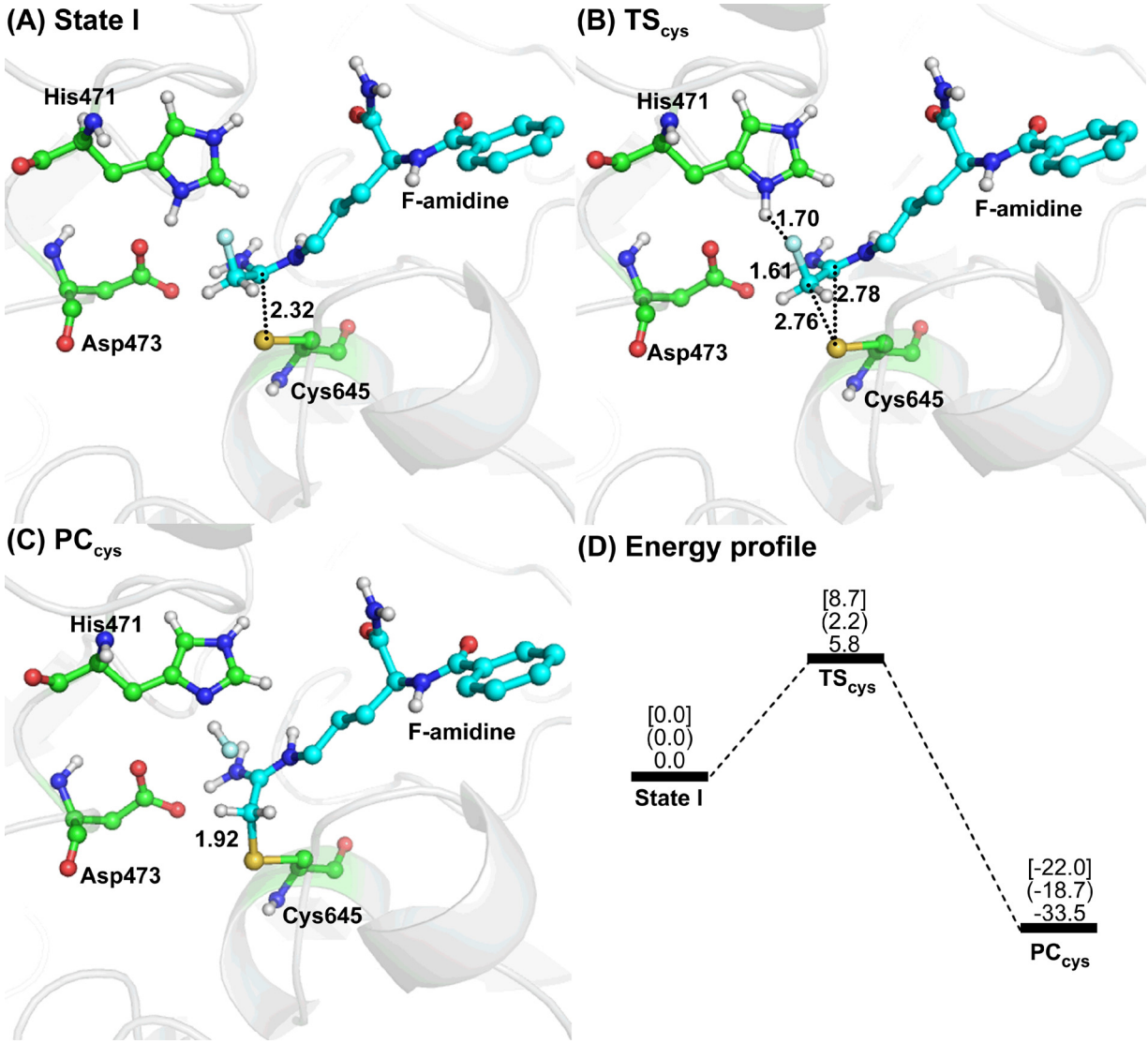

Fig. 6. (A–C) Optimized geometries (bond distances in Å) of key configurations along the inhibition reaction of PAD4 by F-amidine. (D) Energy profile with zero-point corrections for the inhibition reaction.

of 1.61 Å). In the second transition state, TS_2, the proton obtained during the first step transfers from the $O_{\delta 1}$ of Asp473 to the S_γ of Cys645 (with a $O_{\delta 1}$...H distance of 1.25 Å and a H...S_γ distance of 1.70 Å). In the geometry of the final state, where the S_γ of Cys645 is protonated, Asp473 forms two hydrogen bonds with the N_η of F-amidine and the S_γ of Cys645 (with a $O_{\delta 2}$...H—N_η distance of 1.51 Å, and a $O_{\delta 1}$...H—S_γ distance of 2.04 Å). This state corresponds to the neutral state and has similar features as State N in Fig. 3.

As shown in Fig. 4, transformation from State I to State N proceeds in a stepwise manner, the energy barrier for the transformation is 28.3 kcal/mol. State I is much stable than State N, with an energy difference of 19.5 kcal/mol at the ONIOM-EE MP2/6-311++G**:AMBER level. These results confirm that the active site Cys645 exists as a thiolate and that His471 is protonated in the PAD4–F-amidine reactant complex. On the contrary, Zhang and co-workers' QM/MM MD simulation scanned the transformation from State N to State I, and indicated that the State I is less stable than State N (with a free energy difference of 6.0 kcal/mol), the free energy barrier for the transformation is 13.3 kcal/mol. Thus, they suggested that it is unlikely for the active site Cys645 and His471 to be charged in the PAD4 Michaelis reactant complex [40]. In addition, experimental work by Thompson and co-workers revealed that the PAD4 uses a reverse protonation mechanism wherein the active site nucleophile, Cys645, exists as a thiolate in the active form of the enzyme [11]. Our result is inconsistent with Zhang and co-workers' QM/MM MD simulations but is consistent with the reverse protonation mechanism proposed based on the experimental studies by the Thompson group.

3.2. Inhibition reaction mechanism

The inhibition of PAD4 occurs via the initial attack by the Cys645 thiolate on the C_ζ of F-amidine. Fig. 6 illustrates the optimized geometries of State I, transition states (TS_{cys}), and the final product (PC_{cys}). In the QM/MM optimized geometry of State I, the fluoroacetamidine moiety of F-amidine is no longer planar (with a N_ε—C_ζ—C_η—N_η dihedral of 133.9°), indicating that the conjugate system of the fluoroacetamidine is broken. The distance between the S_γ of F-amidine and the C_ζ of PAD4 is 2.32 Å. These results demonstrate that State I is a tetrahedral intermediate similar to the initial tetrahedral intermediate formed during substrate hydrolysis of PAD4. In the transition state TS_{cys}, His471 forms a hydrogen bond with the F of F-amidine (with a N_δ—H...F distance of 1.70 Å) and acts as the proton donor to facilitate the displacement of F from the

C_η of F-amidine. At the same time, the $S_\gamma \ldots C_\zeta$ distance increases to 2.78 Å, and the $S_\gamma \ldots C_\eta$ distance decreases to 2.76 Å, generating a three-membered sulfonium ring. The three-membered ring subsequently opens, and the tetrahedral intermediate collapses, resulting in a 1,2-shift that generates the final thioether adduct PC_{cys}. This product corresponds to the state in the crystal structure (PDB code 2DW5) [17].

We also performed QM/MM calculations on the inhibition mechanism from the structure of State N. The inhibition of PAD4 in State N consists of two reaction steps: (1) the deprotonation of Cys645 by the carboxyl group of Asp473 in concert with the nucleophilic attack by the Cys645 thiolate on the C_ζ of F-amidine, generating a covalent tetrahedral intermediate (see Fig. S2); and (2) the displacement of F from the C_η of F-amidine along with the collapse of the tetrahedral intermediate, resulting in a 1,2-shift that generates the S_γ—C_η covalent bond product (see Fig. S3). The first step is almost barrierless, while the second step is endothermic with a high energy barrier of 59.3 kcal/mol. The high energy barrier of the second step can be attributed to the fact that there is no proton source available to facilitate the displacement of F. In State I, His471 is protonated and can help displace F from the C_η of F-amidine. In contrast, His471 in State N is neutral and cannot aid the displacement of F, leading to the high energy barrier. Thus, the inhibition of PAD4 by F-amidine proceeds predominantly via State I, and His471 acts as a proton donor in the transition state to facilitate the inhibition reaction.

4. Conclusions

We have investigated the mechanism of PAD4 inhibition by F-amidine using a QM/MM approach. We examined two probable states of PAD4: State I and State N. In State I, Cys645 is deprotonated and His471 is charged; in State N, both Cys645 and His471 are neutral. Our calculations indicated that State I can transform to State N through a stepwise manner. In the PAD4–F-amidine reactant complex, State I is 19.5 kcal/mol lower in energy than State N, the active site Cys645 exists as a thiolate, and His471 is protonated. The inhibition of PAD4 by F-amidine is initiated by the nucleophilic addition of S_γ to the C_ζ of F-amidine, leading to the formation of a tetrahedral intermediate. His471 subsequently serves as a proton donor, facilitating the removal of F from the fluoroacetamidine moiety of F-amidine. Meanwhile, S_γ forms a three-membered ring with C_ζ and C_η of F-amidine. Subsequently, the three-membered sulfonium ring collapses and rearranges to generate the final thioether product. The inhibition of PAD4 by F-amidine proceeds predominantly via State I. In the transition state, His471 acts as a proton donor and facilitates the inhibition reaction.

The computationally determined reactant complex of PAD4–F-amidine, the detailed mechanism of PAD4 inhibition by F-amidine, the structure of transition state described in the present study provide a solid base for rational design of mechanism-based PAD4 inhibitors (e.g., substrate analogs with a similar binding mode of F-amidine with PAD4, or stable analogs of the transition-state) and should facilitate the future design of potent compounds in RA treatment and PAD4-targeted ABPPs.

Acknowledgments

This work was supported by National Science Foundation (NSFC, No. 21203101), Specialized Research Fund for the Doctoral Program of Higher Education (SRFDP, No. 20120031120052), Tianjin Natural Science Foundation (No. 14JCQNJC06100) and National Basic Research Program (973 Program, Nos. 2011CBA00800 and 2013CB911100).

Appendix A. Supplementary data

Supplementary data associated with this article can be found, in the online version, at http://dx.doi.org/10.1016/j.jmgm.2014.10.014.

References

[1] E.R. Vossenaar, A.J.W. Zendman, W.J. van Venrooij, G.J.M. Pruijn, PAD, a growing family of citrullinating enzymes: genes, features and involvement in disease, BioEssays 25 (2003) 1106–1118.
[2] K.L. Bicker, P.R. Thompson, The protein arginine deiminases: structure, function, inhibition, and disease, Biopolymers 99 (2013) 155–163.
[3] E. Vossenaar, W. van Venrooij, Citrullinated proteins: sparks that may ignite the fire in rheumatoid arthritis, Arthritis Res. Ther. 6 (2004) 107–111.
[4] C. Foulquier, M. Sebbag, C. Clavel, S. Chapuy-Regaud, R. Al Badine, M.-C. Méchin, C. Vincent, R. Nachat, M. Yamada, H. Takahara, M. Simon, M. Guerrin, G. Serre, Peptidyl arginine deiminase type 2 (PAD-2) and PAD-4 but not PAD-1, PAD-3, and PAD-6 are expressed in rheumatoid arthritis synovium in close association with tissue inflammation, Arthritis Rheum. 56 (2007) 3541–3553.
[5] Y. Wang, J. Wysocka, J. Sayegh, Y.-H. Lee, J.R. Perlin, L. Leonelli, L.S. Sonbuchner, C.H. McDonald, R.G. Cook, Y. Dou, R.G. Roeder, S. Clarke, M.R. Stallcup, C.D. Allis, S.A. Coonrod, Human PAD4 regulates histone arginine methylation levels via demethylimination, Science 306 (2004) 279–283.
[6] J.E. Jones, C.P. Causey, B. Knuckley, J.L. Slack-Noyes, P.R. Thompson, Protein arginine deiminase 4 (PAD4): current understanding and future therapeutic potential, Curr. Opin. Drug Discov. Dev. 12 (2009) 616–627.
[7] A. Galkin, X. Lu, D. Dunaway-Mariano, O. Herzberg, Crystal structures representing the Michaelis complex and the thiouronium reaction intermediate of pseudomonas aeruginosa arginine deiminase, J. Biol. Chem. 280 (2005) 34080–34087.
[8] E.M. Stone, M.D. Person, N.J. Costello, W. Fast, Characterization of a transient covalent adduct formed during dimethylarginine dimethylaminohydrolase catalysis, Biochemistry 44 (2005) 7069–7078.
[9] E.M. Stone, A.L. Costello, D.L. Tierney, W. Fast, Substrate-assisted cysteine deprotonation in the mechanism of dimethylargininase (DDAH) from pseudomonas aeruginosa, Biochemistry 45 (2006) 5618–5630.
[10] P.L. Kearney, M. Bhatia, N.G. Jones, L. Yuan, M.C. Glascock, K.L. Catchings, M. Yamada, P.R. Thompson, Kinetic characterization of protein arginine deiminase 4: a transcriptional corepressor implicated in the onset and progression of rheumatoid arthritis, Biochemistry 44 (2005) 10570–10582.
[11] B. Knuckley, M. Bhatia, P.R. Thompson, Protein arginine deiminase 4: evidence for a reverse protonation mechanism, Biochemistry 46 (2007) 6578–6587.
[12] B. Knuckley, C.P. Causey, J.E. Jones, M. Bhatia, C.J. Dreyton, T.C. Osborne, H. Takahara, P.R. Thompson, Substrate specificity and kinetic studies of PADs 1, 3, and 4 identify potent and selective inhibitors of protein arginine deiminase 3, Biochemistry 49 (2010) 4852–4863.
[13] L.B. Pritzker, M.A. Moscarello, A novel microtubule independent effect of paclitaxel: the inhibition of peptidylarginine deiminase from bovine brain, Biochim. Biophys. Acta 1388 (1998) 154–160.
[14] B. Knuckley, Y. Luo, P.R. Thompson, Profiling protein arginine deiminase 4 (PAD4): a novel screen to identify PAD4 inhibitors, Biorg. Med. Chem. 16 (2008) 739–745.
[15] E.M. Stone, T.H. Schaller, H. Bianchi, M.D. Person, W. Fast, Inactivation of two diverse enzymes in the amidinotransferase superfamily by 2-chloroacetamidine: dimethylargininase and peptidylarginine deiminase, Biochemistry 44 (2005) 13744–13752.
[16] Y. Luo, B. Knuckley, Y.-H. Lee, M.R. Stallcup, P.R. Thompson, A fluoroacetamidine-based inactivator of protein arginine deiminase 4: design, synthesis, and in vitro and in vivo evaluation, J. Am. Chem. Soc. 128 (2006) 1092–1093.
[17] Y. Luo, K. Arita, M. Bhatia, B. Knuckley, Y.-H. Lee, M.R. Stallcup, M. Sato, P.R. Thompson, Inhibitors and inactivators of protein arginine deiminase 4: functional and structural characterization, Biochemistry 45 (2006) 11727–11736.
[18] C.P. Causey, J.E. Jones, J.L. Slack, D. Kamei, L.E. Jones Jr., V. Subramanian, B. Knuckley, P. Ebrahimi, A.A. Chumanevich, Y. Luo, H. Hashimoto, M. Sato, L.J. Hofseth, P.R. Thompson, The development of N-α-(2-carboxyl)benzoyl-N^5-(2-fluoro-1-iminoethyl)-L-ornithine amide (o-F-amidine) and N-α-(2-carboxyl) benzoyl-N^5-(2-chloro-1-iminoethyl)-L-ornithine amide (o-Cl-amidine) as second generation protein arginine deiminase (PAD) inhibitors, J. Med. Chem. 54 (2011) 6919–6935.
[19] J.E. Jones, J.L. Slack, P. Fang, X. Zhang, V. Subramanian, C.P. Causey, S.A. Coonrod, M. Guo, P.R. Thompson, Synthesis and screening of a haloacetamidine containing library to identify PAD4 selective inhibitors, ACS Chem. Biol. 7 (2012) 160–165.
[20] V.C. Willis, A.M. Gizinski, N.K. Banda, C.P. Causey, B. Knuckley, K.N. Cordova, Y. Luo, B. Levitt, M. Glogowska, P. Chandra, L. Kulik, W.H. Robinson, W.P. Arend, P.R. Thompson, V.M. Holers, N-α-benzoyl-N5-(2-chloro-1-iminoethyl)-l-ornithine amide, a protein arginine deiminase inhibitor, reduces the severity of murine collagen-induced arthritis, J. Immunol. 186 (2011) 4396–4404.
[21] Y. Wang, P. Li, S. Wang, J. Hu, X.A. Chen, J. Wu, M. Fisher, K. Oshaben, N. Zhao, Y. Gu, D. Wang, G. Chen, Y. Wang, Anticancer peptidylarginine deiminase (PAD)

inhibitors regulate the autophagy flux and the mammalian target of rapamycin complex 1 activity, J. Biol. Chem. 287 (2012) 25941–25953.
[22] Y. Luo, B. Knuckley, M. Bhatia, P.J. Pellechia, P.R. Thompson, Activity-based protein profiling reagents for protein arginine deiminase 4 (PAD4): synthesis and in vitro evaluation of a fluorescently labeled probe, J. Am. Chem. Soc. 128 (2006) 14468–14469.
[23] B. Knuckley, C.P. Causey, P.J. Pellechia, P.F. Cook, P.R. Thompson, Haloacetamidine-based inactivators of protein arginine deiminase 4 (PAD4): evidence that general acid catalysis promotes efficient inactivation, ChemBioChem 11 (2010) 161–165.
[24] K. Arita, T. Shimizu, H. Hashimoto, Y. Hidaka, M. Yamada, M. Sato, Structural basis for histone N-terminal recognition by human peptidylarginine deiminase 4, Proc. Natl. Acad. Sci. U.S.A. 103 (2006) 5291–5296.
[25] D.A. Case, et al., Amber 11, University of California, San Francisco, 2010.
[26] M.J. Frisch, et al., Gaussian 03, Revision C.02, Gaussian, Inc, Wallingford, CT, 2004.
[27] J. Wang, W. Wang, P.A. Kollman, D.A. Case, Automatic atom type and bond type perception in molecular mechanical calculations, J. Mol. Graph. Model 25 (2006) 247–260.
[28] C. Lee, W. Yang, R.G. Parr, Development of the Colle-Salvetti correlation-energy formula into a functional of the electron density, Phys. Rev. B 37 (1988) 785–789.
[29] A.D. Becke, Density-functional thermochemistry. III. The role of exact exchange, J. Chem. Phys. 98 (1993) 5648–5652.
[30] P.J. Stephens, F.J. Devlin, C.F. Chabalowski, M.J. Frisch, Ab initio calculation of vibrational absorption and circular dichroism spectra using density functional force fields, J. Phys. Chem. 98 (1994) 11623–11627.
[31] W.D. Cornell, P. Cieplak, C.I. Bayly, I.R. Gould, K.M. Merz, D.M. Ferguson, D.C. Spellmeyer, T. Fox, J.W. Caldwell, P.A. Kollman, A second generation force field for the simulation of proteins, nucleic acids, and organic molecules, J. Am. Chem. Soc. 117 (1995) 5179–5197.
[32] V. Hornak, R. Abel, A. Okur, B. Strockbine, A. Roitberg, C. Simmerling, Comparison of multiple amber force fields and development of improved protein backbone parameters, Proteins 65 (2006) 712–725.
[33] J. Wang, R.M. Wolf, J.W. Caldwell, P.A. Kollman, D.A. Case, Development and testing of a general Amber force field, J. Comput. Chem. 25 (2004) 1157–1174.
[34] J.-P. Ryckaert, G. Ciccotti, H.J.C. Berendsen, Numerical integration of the Cartesian equations of motion of a system with constraints: molecular dynamics of n-alkanes, J. Comput. Phys. 23 (1977) 327–341.
[35] U. Essmann, L. Perera, M.L. Berkowitz, T. Darden, H. Lee, L.G. Pedersen, A smooth particle mesh Ewald method, J. Chem. Phys. 103 (1995) 8577–8593.
[36] F. Maseras, K. Morokuma, IMOMM: a new integrated ab initio + molecular mechanics geometry optimization scheme of equilibrium structures and transition states, J. Comput. Chem. 16 (1995) 1170–1179.
[37] M. Svensson, S. Humbel, R.D.J. Froese, T. Matsubara, S. Sieber, K. Morokuma, ONIOM: a multilayered integrated MO + MM method for geometry optimizations and single point energy predictions. A test for Diels–Alder reactions and $Pt(P(t\text{-}Bu)_3)_2 + H_2$ oxidative addition, J. Phys. Chem. 100 (1996) 19357–19363.
[38] T. Vreven, K.S. Byun, I. Komáromi, S. Dapprich, J.A. Montgomery, K. Morokuma, M.J. Frisch, Combining quantum mechanics methods with molecular mechanics methods in ONIOM, J. Chem. Theory Comput. 2 (2006) 815–826.
[39] M.J. Frisch, et al., Gaussian 09, Revision A.01, Gaussian, Inc., Wallingford, CT, 2009.
[40] Z. Ke, Y. Zhou, P. Hu, S. Wang, D. Xie, Y. Zhang, Active site cysteine is protonated in the PAD4 Michaelis complex: evidence from Born-Oppenheimer ab initio QM/MM molecular dynamics simulations, J. Phys. Chem. B 113 (2009) 12750–12758.
[41] Z. Ke, S. Wang, D. Xie, Y. Zhang, Born-Oppenheimer ab Initio QM/MM molecular dynamics simulations of the hydrolysis reaction catalyzed by protein arginine deiminase 4, J. Phys. Chem. B 113 (2009) 16705–16710.
[42] K. Arita, H. Hashimoto, T. Shimizu, K. Nakashima, M. Yamada, M. Sato, Structural basis for Ca^{2+}-induced activation of human PAD4, Nat. Struct. Mol. Biol. 11 (2004) 777–783.